



**HAL**  
open science

## Quantification and Prediction of the 3D Pore Network Evolution in Carbonate Reservoir Rocks

Eva de Boever, Clément Varloteaux, Fadi H. Nader, Anneleen Foubert, Samir Bekri, Souhail Youssef, Elisabeth Rosenberg

► **To cite this version:**

Eva de Boever, Clément Varloteaux, Fadi H. Nader, Anneleen Foubert, Samir Bekri, et al..  
Quantification and Prediction of the 3D Pore Network Evolution in Carbonate Reservoir Rocks.  
Oil & Gas Science and Technology - Revue d'IFP Energies nouvelles, 2012, 67 (1), pp.161-178.  
10.2516/ogst/2011170 . hal-00702951

**HAL Id: hal-00702951**

**<https://ifp.hal.science/hal-00702951>**

Submitted on 31 May 2012

**HAL** is a multi-disciplinary open access archive for the deposit and dissemination of scientific research documents, whether they are published or not. The documents may come from teaching and research institutions in France or abroad, or from public or private research centers.

L'archive ouverte pluridisciplinaire **HAL**, est destinée au dépôt et à la diffusion de documents scientifiques de niveau recherche, publiés ou non, émanant des établissements d'enseignement et de recherche français ou étrangers, des laboratoires publics ou privés.

# Quantification and Prediction of the 3D Pore Network Evolution in Carbonate Reservoir Rocks

E. De Boever<sup>1\*#</sup>, C. Varloteaux<sup>1</sup>, F.H. Nader<sup>1</sup>, A. Foubert<sup>2</sup>, S. Békri<sup>1</sup>,  
S. Youssef<sup>1</sup> and E. Rosenberg<sup>1</sup>

<sup>1</sup> IFP Energies nouvelles, 1-4 avenue de Bois-Préau, 92852 Rueil-Malmaison Cedex - France

<sup>2</sup> K.U.Leuven, Dept. of Earth and Environmental Sciences, Celestijnenlaan 200E, 3001 Heverlee - Belgium

e-mail: eva.deboever@vito.be - clement.varloteaux@ifpen.fr - fadi-henri.nader@ifpen.fr - anneleen.foubert@ees.kuleuven.be  
samir.bekri@ifpen.fr - souhail.youssef@ifpen.fr - elisabeth.rosenberg@ifpen.fr

\* Corresponding author

# Current address: VITO NV, Unit Raw Materials, Boeretang 200, 2400 Mol - Belgium

## Résumé — Quantification et prédiction de l'évolution d'un réseau 3D de pores dans des roches réservoirs de carbonates

— Cette étude présente une approche intégrée qui permet la reconstruction et la prédiction des modifications de structure 3D de pores ainsi que le développement de la porosité/perméabilité tout au long de la diagenèse des carbonates. Des modèles de réseau de pores réactifs peuvent prédire les changements en matière de propriétés de transport de milieux poreux, résultant des phénomènes de dissolution/cimentation. La validité et prédictibilité de ces modèles dépendent toutefois de la représentativité des réseaux de pores équivalents utilisés et des équations et paramètres utilisés pour modéliser les événements diagénétiques. L'approche développée est appliquée au cas réel d'une roche dolomitique de la formation arabe moyen orientale. La microscopie 2D standard montre que le processus principal affectant la qualité de réservoir consiste en la dolomitisation, suivie d'un renforcement de la porosité dû à une dissolution de la dolomie et à une destruction de la porosité secondaire par cimentation de l'anhydrite diagénétique tardive. La microtomographie par rayons X informatisée (*X-ray  $\mu$ -CT*; *X-ray computer (micro)tomography*) permet de quantifier le volume et la distribution en 3D des différents constituants d'échantillon. Les résultats sont comparés avec les mesures de laboratoire. Des réseaux de pores équivalents avant la dissolution dolomitique et préalablement à la précipitation d'anhydrite tardive sont reconstruits et utilisés pour simuler les caractéristiques de porosité, de perméabilité lors de ces étapes diagénétiques. En utilisant ces structures 3D de pores, la PNM-R (*Pore Network Modeling Reactive*; modélisation réactive de réseau de pores) peut suivre les voies d'évolution plausible de porosité-perméabilité entre ces étapes. Les conditions d'écoulement et les vitesses de réaction obtenues par modélisation des voies de réaction géochimiques peuvent être utilisées en tant que référence pour définir les paramètres de modèle de PNM-R. L'approche peut être utilisée pour un typage dynamique de roches et le passage à une échelle supérieure de propriétés pétrophysiques, nécessaires pour la modélisation de réservoir.

## Abstract — Quantification and Prediction of the 3D Pore Network Evolution in Carbonate Reservoir Rocks

— This study presents an integrated approach that allows the reconstruction and prediction of 3D pore structure modifications and porosity/permeability development throughout carbonate diagenesis. Reactive Pore Network Models (PNM-R) can predict changes in the transport properties of porous media, resulting from dissolution/cementation phenomena. The validity and predictability of these models however depend on the representativeness of the equivalent pore networks used and on the equations and parameters used to model the diagenetic events. The developed approach is applied to a real case of a

*dolostone rock of the Middle East Arab Formation. Standard 2D microscopy shows that the main process affecting the reservoir quality is dolomitisation, followed by porosity enhancement due to dolomite dissolution and secondary porosity destruction by cementation of late diagenetic anhydrite. X-ray  $\mu$ -CT allows quantifying the 3D volume and distribution of the different sample constituents. Results are compared with lab measurements. Equivalent pore networks before dolomite dissolution and prior to late anhydrite precipitation are reconstructed and used to simulate the porosity, permeability characteristics at these diagenetic steps. Using these 3D pore structures, PNM-R can trace plausible porosity-permeability evolution paths between these steps. The flow conditions and reaction rates obtained by geochemical reaction path modeling can be used as reference to define PNM-R model parameters. The approach can be used in dynamic rock typing and the upscaling of petrophysical properties, necessary for reservoir modeling.*

## INTRODUCTION

Carbonates hold about half of the world's oil and gas reservoirs. Porous and permeable carbonate reservoir rocks are however known to be heterogeneous in terms of the spatial distribution of their petrophysical properties, which makes production and secondary recovery a challenging task (Ehrenberg, 2006; Lucia, 2007). The pore structure is, in the first place, controlled by the distribution of depositional textures, but it is most often strongly modified during diagenesis. Different phases of cementation, dissolution and replacement processes like dolomitisation may successively create, destroy or redistribute the pore space available for oil, gas, water or CO<sub>2</sub> storage. This often results in the presence of multiple pore systems that are variously interconnected. Difficulties, typically, arise when rock-types and reservoir properties are to be defined and predicted.

Moreover, understanding how diagenetic processes affected the pore structure, the quantification of these phenomena and accompanying changes in petrophysical properties are essential for a reliable prediction of reservoir quality as it can assist in understanding and quantifying the evolution of different reservoir rock-types throughout their diagenetic history. X-ray computer (micro)tomography ( $\mu$ -CT) offers a tool to image and quantify the 3D rock fabric and describe in detail complex pore network geometries. In addition to these techniques, available numerical tools can be used to simulate the evolution of petrophysical rock properties.

The numerical tool that is used in this study to model the consequence of dissolution or cementation on petrophysical rock properties is based on Pore Network Modeling (PNM). This approach provides a way of correctly describing the pore scale phenomena by using well-known continuum equations. The problem can then be upscaled to the core scale by calculating effective and global properties (Algive *et al.*, 2009b). The Pore Network Model is a conceptual representation of a porous medium. The pore structure is modeled by a three-dimensional network of pore bodies (nodes) interconnected by pore throats (bonds). In this way, the topology effects (connectivity, aspect ratio, tortuosity) are easily considered. This is undoubtedly an advantage compared with the

pioneering models of reactive transport, based on randomly distributed capillaries (Schechter and Gidley, 1969; Christman and Edgar, 1983), which failed to predict the impacts of surface reactions in the presence of flow. The PNM approach, initially developed to study multiphase flow (Fatt, 1956), has been successfully applied to a gaseous, reactive flow in catalysis (Rieckmann and Frerich, 1997). In this case, the concentration can be reasonably considered as uniform at the pore scale and the catalyst structure remains unchanged. However, such assumptions are no longer valid when dealing with surface reaction, such as dissolution and precipitation mechanisms. The local concentration profile and the pore structure variations must be taken into account when solving the governing equations. Reactive-PNMs (PNM-R) have been applied to predict porosity-permeability changes during and following the injection of CO<sub>2</sub> or its geological storage in aquifers (Li *et al.*, 2006; Algive *et al.*, 2009b; Bemer and Lombard, 2010; Izgec *et al.*, 2010). In contrast, the application and validation of PNM-R in studies of the evolution of reservoir rock properties during early and late diagenetic processes, remain yet poorly explored, though of interest for reservoir modeling.

This pilot study demonstrates an approach for the simulation of changes in petrophysical properties during dissolution/precipitation phenomena that affected a carbonate reservoir rock during diagenesis. Simulations start from reconstructions of the real 3D pore structure using  $\mu$ -CT at different diagenetic time steps. The validity of the results will be discussed by comparing them with lab measurements and results of geochemical reaction path modeling. The studied case consists of a dolostone well core sample of the Jurassic Arab Formation being representative of an excellent gas reservoir in the Arabian Gulf region.

## 1 GEOLOGICAL BACKGROUND OF SAMPLE

The rock sample is a dolostone of the Arab C member (*Fig. 1*). The Upper Jurassic Arab Formation is geographically widespread in the Arabian Gulf region and consists of four carbonate-evaporite cycles (or members), A to D, from top down.

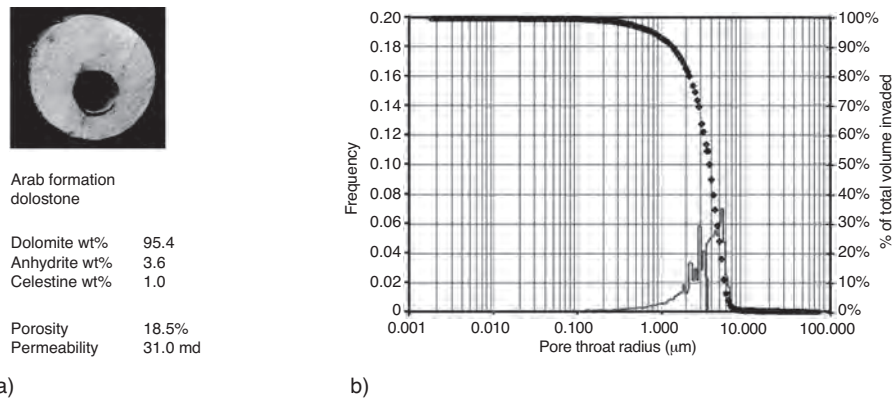


Figure 1

a) Image of sample plug (diameter 23 mm), quantitative XRD data and porosity, permeability results on plug sample;  
 b) Pore size distribution as derived from mercury intrusion experiments on plug material.

They reflect cyclic deposition in a progressively shallowing, marginal marine shelf to sabkha environment of a wide ramp. The Arab C and D members constitute the reservoirs of the Arab Formation (Cantrell and Hagerty, 2003; Lindsay *et al.*, 2006), whereas the Arab A and B members comprise overall non-reservoir rocks due to an increase in evaporative deposition that grade into the overlying Hith Formation. The latter chiefly consists of anhydrite with minor dolostones and acts as a seal for several reservoirs in the Arab Formation (Alsharhan, 1989).

Relevant reservoir rock characterization studies on the Middle East Arab Formation have been carried out by other authors (Mitchell *et al.*, 1988; Meyer and Price, 1992; Cantrell and Hagerty, 2003; Lindsay *et al.*, 2006; Ehrenberg *et al.*, 2007) of which few report on the diagenetic and burial history (Swart *et al.*, 2005; Morad *et al.*, accepted) providing the necessary background data for this advanced, quantitative study. The Arab Formation in the study region is progradational, interrupted by several steps of increased subsidence rates until the Late Cretaceous when the obduction of the Oman ophiolites slowed down the burial rate. The Jurassic Diyab Formation is probably a major oil source rock (Alsharhan, 1989) and achieved peak oil generation and migration during the Eocene.

## 2 METHODOLOGY

### 2.1 Geological Sample Characterization

The studied sample is rather homogeneous on the millimetre-scale, encloses different mineral phases and possesses an elevated porosity and permeability, facilitating a PNM study. Thin sections, half-stained for carbonates with Alazarin Red S and K-ferricyanide and impregnated with a blue resin are studied petrographically (standard transmitted light and

fluorescence microscopy). Conventional 2D petrography allows identification of the nature and succession of diagenetic phases and the evolution of porosity.

About 4 g of bulk sample is finely grinded in an agate mortar for quantitative X-ray diffraction (XRD) measurements. This technique allows the quantification of mineral abundances in terms of their weight percentage (wt%) and measurements can be used as calibration for the quantification results obtained from  $\mu$ -CT images. Sample preparation and XRD measurements are carried out according to the procedure described by Snellings *et al.* (2010). A Phillips PW1830 device is used with a  $\text{CuK}\alpha_{1,2}$  radiation at 30 mA and 45 kV and graphite monochromator and a gas proportional scintillation detector. Diffractometer scans are recorded in the Bragg-Brentano geometry ( $5$  to  $70^\circ$   $2\theta$ , step size  $0.02^\circ$   $2\theta$ , 2 s counting time per step). Phase quantification includes a phase identification step using the DiffracPlus EVA software (Bruker) and a quantitative phase analysis step by the full profile Rietveld method (Topas Academic v4.1 software; Coelho, 2007). Uncertainty (standard deviation) of the Rietveld method is 3 wt%. The analysis of multiple subsamples of a single plug show a maximum standard deviation of 1.5 wt%.

### 2.2 Computer Tomography (CT) Analysis

#### 2.2.1 $\mu$ -CT Setup and Image Reconstruction

Following a  $\mu$ -CT scan of the 23 mm diameter core sample, a representative miniplug of 5 mm diameter is drilled. A 3D view of a plug is acquired using a Nanotom high resolution X-ray  $\mu$ -CT from PHOENIX X-Ray, installed at IFP Energies nouvelles. 2D projections are realised by rotating the sample over  $360^\circ$  at rotation steps of  $0.2^\circ$ . Parameters during acquisition are a tube voltage of 90 kV and a current of 170  $\mu\text{A}$ . The detector is a Hamamatsu flat detector

(110 mm × 110 mm) made up of a 2304 × 2304 pixels grid, with a step of 50 μm. The source-object distance is 11.8 mm and the source-detector distance 200 mm, providing a resolution of 3 μm (pixel size). The presence of small pores and pore throats however required a lower pixel size. To increase the resolution, the detector was shifted along the projection plan to create a virtual detector of 2304 × 4608 pixels (pxls), allowing a larger field of view. The source-object distance is adjusted to 6.2 mm to double the magnification ratio. With this set up the resulting resolution is 1.5 μm. In counterpart, the acquired data size and the acquisition time double. Each acquisition generates 1800 TIFF projections that are used for the numerical reconstruction of volumetric data. The maximum volume that can be reconstructed and stored at full resolution is 1000 × 1000 × 1000. The reconstruction (PHOENIX algorithm) uses a cone beam Feldkamp algorithm. The beam hardening effect is corrected by using a metal Cu-filter (0.1 mm) and a mathematical correction during the reconstruction process.

### 2.2.2 3D Quantification and Building an Equivalent Pore Network

The workflow for image treatment and analysis of the reconstructed 3D volumes consists of:

- visualizing, isolating and quantifying the resolved pore space and different mineral phases;
- the reconstruction of an equivalent pore network and description of its parameters, and;
- the reconstruction of ancient pore networks.

The volume is visualized and analyzed using the Avizo software package (version 6.2, VSG, France) and ImageJ software 1.44. In order to reduce noise and increase image contrast, the image histograms are stretched and the images are filtered if appropriate (application of mean, brightness/contrast filter). Segmentation of the gray level image to accurately separate each gray class one by one includes a thresholding step, followed by additional filtering operations (removal of islands) and morphological operations (smoothing, shrinking and growing). More details can be found in Youssef *et al.* (2008). This creates a binary 3D image of each phase and allows calculating the volumetric percentages of the sample constituents and visualizing their spatial distribution. The quality of the image segmentation can be evaluated by comparing the calculated volumetric percentages with classical He-porosity values and quantitative XRD results on adjacent plug material. The 3D pore space is typically composed of several, independent pore clusters. To further proceed, the pore space should include at least one, important percolating porosity cluster to acquire representative results during PNM.

Step 2 and 3 of the image treatment procedure are described in detail by Youssef *et al.* (2007a, b). When the different pores are geometrically separated and labelled

several statistical parameters of the equivalent pore network can be defined, *e.g.* the pore size distribution, pore radii and the coordination number of each pore.

In a last step, ancient pore networks are reconstructed from the μ-CT images. The procedure consists of an additional segmentation and pore network building step analogous to the procedure outlined above. The segmentation step involves a double thresholding operation. The present pore space is isolated and merged with the segmented volume of a second mineral phase, *e.g.* anhydrite, that plugs part of the actual porosity.

### 2.3 Numerical Simulation of Mercury Intrusion and Permeability

Following pore space partitioning for present and ancient pore networks, a connection matrix is built that is used to simulate mercury intrusion and calculate the permeability. A full drainage curve is obtained by a step by step invasion of an entire pore volume that is accessible via its throat radius for a fixed capillary pressure ( $P_c$ ). The procedure is explained in detail by Youssef *et al.* (2007b). Comparison of simulation results for the actual pore space with lab permeability and Purcell mercury porosimetry measurements on adjacent material is used to validate the quality of the reconstructed pore network.

### 2.4 Geochemical Reaction Path Modeling

To obtain an estimate of dissolution and precipitation rates, the evolution of an open geochemical system, changing at a rate governed by the fluid and rock composition and reaction kinetics is modeled. Arxim software (EMSE, France) is an open source program for multiphase speciation, equilibrium and reaction calculations between minerals, aqueous solutions and gases. The reactions take place in a box with the size of a small plug (2.5 cm<sup>3</sup>) since we are looking at processes at this scale. The geochemical calculations include the solid phases dolomite, calcite, anhydrite and porosity in volume% as obtained from quantitative XRD, He-porosimetry data and μ-CT images. The reactive surface area is calculated by Arxim, based on the grain (or “crystal”) radius, using a floating sphere textural model for mineral representation. Grain radii are estimated from thin section observations. The reactive surface area is derived by assuming that the crystal radius is the radius of a sphere and taking into account the volume of the minerals in the studied box (2.5 cm<sup>3</sup>). The size of the spheres varies as mineral reactions progress and account for variations of mineral surface and permeability. The reactive surface area is an important input parameter when kinetic mineral reactions are considered, but it remains poorly constrained (see Brosse *et al.*, 2005). The outlined approach, starting from a sphere textural model, produces only a rough

estimate of the total pore surface available for reaction and in contact with the fluid flow. It does not include the nonspherical character of the crystals and does not account for the roughness of the mineral surface. A sensitivity study shows that with a one order change in the reactive surface area, the intrinsic rate constant of the reaction (parameter  $\kappa$  in Eq. 3) changes with one order.

Fluid compositions are described by their pH and the concentration (mol/kg) of 7 components involved in calcite-dolomite-anhydrite reactions. The compositions of fluids in equilibrium with the rock assemblage, used as a basis in the calculations, are listed in Table 1. Ionic strength of formation waters are higher than 3.0 and Pitzer (1973) equations are used in speciation/equilibrium calculations. The USGS database (Palandri and Kharaka, 2004) is used for the kinetic constants in Arxim.

Background information on the geological history serves to constrain the timing, pressure ( $P$ ) and temperature ( $T$ ) during which different cementation/dissolution events took place. Advective fluid flow velocities were varied between 0.002 m/y and 0.5 m/y. Constraints on flow velocities were derived from Whitaker *et al.* (2004) who give an interesting overview of the flow velocities of basin-scale fluid movements resulting from a range of driving forces. A one order increase or decrease in flow velocity results in a one to two order change in the intrinsic rate constant (Eq. 3).

The simulations represent thermodynamic-kinetic reaction path calculations in a box with length  $dx$  (m), on which an advective flow is imposed. During dynamic simulations, a fluid is injected that is out of equilibrium as a result of small

changes in the fluid chemistry ( $Mg^{2+}$ ,  $Ca^{2+}$ ,  $SO_4^{2-}$ ,  $CO_2$  concentration or salinity) and/or temperature. Temperature and pressure conditions during one run are constant. Because of the uncertainties associated with the fluid composition and reaction conditions; the parameters  $T$ ,  $P$  and fluid composition ( $Mg^{2+}$ ,  $Ca^{2+}$ ,  $SO_4^{2-}$ ,  $CO_2$  concentration and salinity) were in addition changed as part of a sensitivity study. A closed system run allows determining the equilibration time of the fluid with the rock. The advective velocities implied during open system, dynamic runs are chosen as such that the fluid leaves the volume, with length  $dx$ , prior to equilibration.

Envisaging the implementation of the calculated reaction rates in a reactive pore network model that can address only one reaction, each simulation addresses one dissolution or precipitation reaction. The results therefore reflect a simplified geological situation. Each diagenetic process is simulated, according to one or more scenarios. The scenarios are selected, based on detailed work on the Arab C Formation and on background literature of the geological history of the study area (Mitchell *et al.*, 1988; Meyer and Price, 1992; Cantrell and Hagerty, 2003; Swart *et al.*, 2005; Lindsay *et al.*, 2006; Ehrenberg *et al.*, 2007; Morad *et al.*, accepted). The maximum geological duration of the diagenetic events (in My) is derived from the burial curve of the study area (Morad *et al.*, accepted) and aids in eliminating unrealistic scenarios.

The volume that is dissolved/precipitated during reaction is obtained from  $\mu$ -CT images. The reaction rates and flow velocities obtained by geochemical modeling are compared to and used as a reference for the Peclet (Eq. 2, see below) and Peclet-Damköhler number (Eq. 3, see below) in the PNM-R. The calculated reaction rates (volume dissolved/precipitated per time unit) reflect the rate of dissolution/precipitation in a realistic geochemical space, but can not account for heterogeneities at the pore scale and changes in the fluid path. The 3D volume of dissolution or cementation, obtained from CT images and the maximum geological duration of the diagenetic event (in My), as described in literature, demonstrate the necessity to study far-from-equilibrium geochemical systems in order to achieve sufficiently fast reaction progress with time.

TABLE 1

Geochemical composition of fluids in equilibrium with the host rock at the given temperature and pressure that mark the onset of the diagenetic process (dolomite dissolution or anhydrite precipitation).

The concentrations of geochemical components is based on formation water data from the Arab Formation (Morad *et al.*, accepted), brine compositions in equilibrium with the Smackover Formation (Moldovanyi *et al.*, 1992) and surface Abu Dhabi sabkha waters (Wood *et al.*, 2002). During each reaction path simulation, one or a combination of these parameters is varied (see Tab. 4)

Component (mol/kg)	Dolomite dissolution		Anhydrite precipitation	
Cl <sup>-</sup>	3.3	3.3	3.3	
SO <sub>4</sub> <sup>2-</sup>	0.051	0.047	0.054	
CO <sub>2</sub> (aq)	0.0077	0.0268	0.0020	
Na <sup>+</sup>	3.381	3.372	3.390	
K <sup>+</sup>	0.01	0.01	0.01	
Mg <sup>2+</sup>	0.00014	0.00092	0.00066	
Ca <sup>2+</sup>	0.0089	0.0061	0.0044	
pH	6.5	5.7	6.4	
Temperature (°C)	85	95	95	

## 2.5 Reactive Pore Network Modeling (PNM-R)

The PNM technique was originally developed to calculate multiphase flow properties of a porous medium (*e.g.* relative permeabilities, capillary pressure, resistivity index) from a pore structure characterization. It can account for various phenomena occurring at pore scale and was therefore also found appropriate to identify the change in structure caused by the dissolution/precipitation mechanisms (Algive *et al.*, 2009a) and the consequences on petrophysical properties (porosity and permeability). Using the pore network approach has the

advantage of reflecting the structure key characteristics (connectivity, tortuosity, etc.) while simplifying the geometry features. The pore throats are modeled by basic geometries, such as cylindrical, triangular and elliptical capillaries, whereas the pore-bodies are represented by spheres or cubes. Thus, in each element (pore body or throat), the reactive transport can easily be upscaled and the scale factors determined, according to the microscopic dimensionless numbers of Peclet and Peclet-Damköhler (Algive *et al.*, 2009b).

The used Reactive Pore Network Model can be divided into three main tasks. Firstly, the reactive transport scale factors ( $\gamma^*$ ,  $v^*$  and  $D^*$ ) must be determined for each basic geometry used in PNM. Secondly, the concentration field can be determined analytically by:

- solving the macroscopic reactive transport Equation (1) in each throat and;
- doing a mass balance nearby each pore of the network. Finally, the structural modifications and their impacts on petrophysical properties are computed.

$$\frac{\partial \bar{c}'}{\partial t} + \nabla \cdot (\bar{v}^* \bar{c}' - \bar{D}^* \cdot \nabla \bar{c}') + \bar{\gamma}^* \bar{c}' = 0 \quad (1)$$

with  $c' = \frac{c - c^*}{\bar{c}_0 - c^*}$

where  $\bar{c}'$  is the normalized mean chemical disequilibrium of the element (*i.e.* pore body or pore throat in a Pore Network Model). Three macroscopic coefficients appear in the previous transport equation:

- $\bar{\gamma}^*$  the volumetric apparent reaction rate coefficient, which takes into account source/sink terms due to surface and possibly volume reactions;
- $\bar{v}^*$  the macroscopic velocity vector of the solute, different from the mean velocity of the fluid because of reactions;
- $\bar{D}^*$  the dispersive tensor, which is not equal to the classical Taylor-Aris dispersion.

The pore size distribution before and after reaction can be compared to qualitative observations and quantitative  $\mu$ -CT results. Furthermore, background geological information and reaction rates obtained from geochemical simulations can be used to constrain the pore network modeling conditions and parameters. It is, in fact, possible to estimate the above-mentioned dimensionless numbers of Peclet ( $Pe$ ) and Peclet-Damköhler ( $PeDa$ ) that define the regime of dissolution/precipitation in which the system will evolve from the geochemical simulation results. The Peclet number is defined as the ratio of convection to diffusion time. The  $PeDa$  number compares the diffusion and intrinsic reaction characteristic times:

$$Pe = \frac{\bar{v}l}{D} \quad (2) \quad \text{and} \quad PeDa = \frac{\kappa l}{D} \quad (3)$$

where  $\bar{v}$  is the Darcy flow rate,  $l$  the mean radius over the network,  $D$  the molecular diffusion and  $\kappa$  the intrinsic rate constant of the surface reaction.

More details on the PNM-R characteristics and construction are provided in Laroche and Vizika (2005). At first, this model has been developed for three-dimensionnal cubic lattice networks. With the progress of the reconstruction algorithm and  $\mu$ -CT resolution, this model has been generalized to the use of equivalent, complex networks. Such a network provides a better understanding of the porous media structure and its consequences on dissolution/precipitation patterns.

### 3 APPLICATION TO ARAB C DOLOSTONE

#### 3.1 Diagenesis

The studied Arab C dolostone rock consists of subhedral to euhedral dolomite rhombs (20-100  $\mu$ m diameter), building a homogeneous fabric with intercrystalline microporosity and minor moldic and vuggy porosity (Lønøy, 2006) (*Fig. 2a*). The present porosity constitutes 18.5% (*Fig. 1*). The process of early dolomitisation is non-fabric preserving. A transparent, euhedral dolomite cement occurs as rims around the cloudy, inclusion-rich replacement dolomite or as euhedral rhombs in intercrystalline porosity (*Fig. 2b*). Minor moldic porosity is the result of dissolution of previous, unstable carbonate grains. Some larger, irregular vuggy pores also exist between dolomite crystals suggesting a dolomite dissolution event prior to late anhydrite cementation (crystal size: 200-400  $\mu$ m; *Fig. 2b, c*). Anhydrite crystals replace dolomite in places. The late anhydrite phase suffered from alteration and is locally surrounded by celestine. The latter is only visible in reconstructed  $\mu$ -CT images and not in the available thin section. Minor patches of late poikilotopic calcite fill, in places, intercrystalline porosity.

The present reservoir properties chiefly reflect diagenetic modifications postdating sediment deposition, *i.e.* dolomitisation-dolomite cementation creating a connected intercrystalline pore network, followed by minor dolomite dissolution and finally anhydrite cementation/replacement. These different steps in the diagenetic history of the rock sample are illustrated in Figure 3. In the following, we will focus on three relevant diagenetic time steps. Time 0 represents the original, intercrystalline pore structure following dolomitisation. Time 1 refers to the pore structure following dolomite dissolution, prior to anhydrite cementation/replacement. Time 2 refers to the actual pore structure following anhydrite replacement and cementation.

#### 3.2 Equivalent Pore Network Reconstruction and Numerical Transport Simulation

The fabric of the dolostone appears homogeneous in CT images of the 23 mm and 5 mm diameter plug. Two adjacent  $1\,000 \times 1\,000 \times 1\,000$  pixels volumes were extracted from the miniplug (resolution 1.5  $\mu$ m, total volume: 6.7 mm<sup>3</sup>). The porosity% was calculated for several volumes of increasing

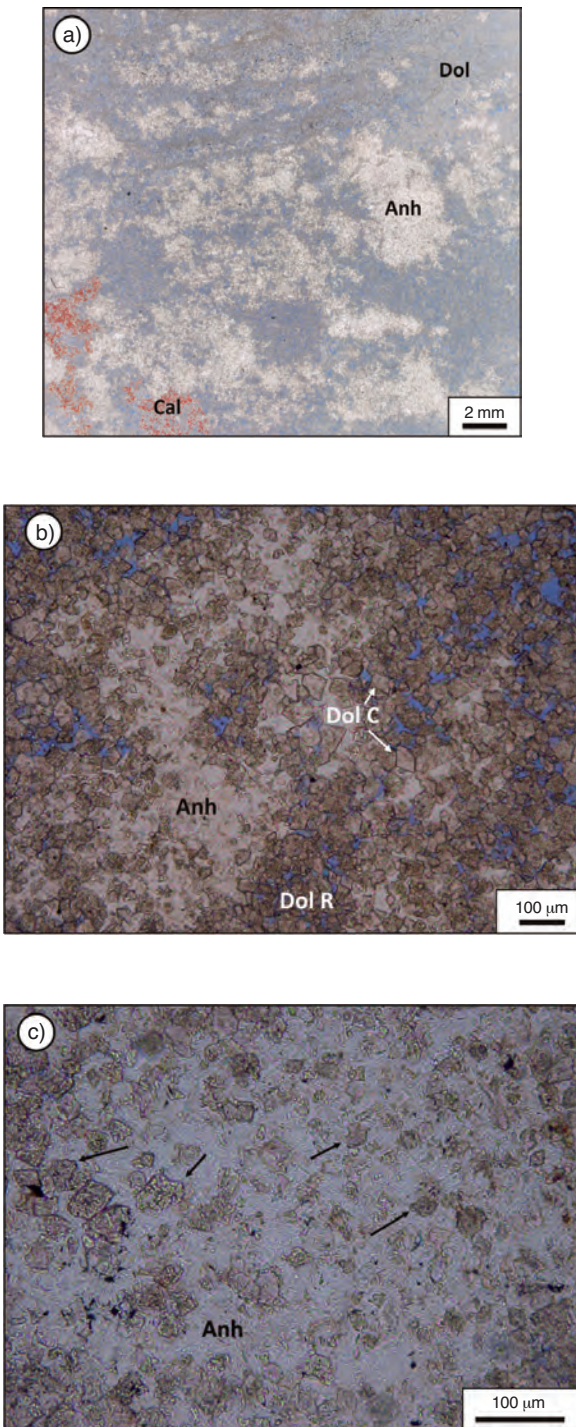


Figure 2

a) Overview transmitted light microscopic image of stained dolostone sample. Anh = anhydrite, Calc = calcite, Dol = dolomite; b) Detailed transmitted light microscopic image showing the dolostone fabric. Anh = anhydrite, Dol R = replacive dolomite, Dol C = dolomite cement; c) Detail with arrows indicating partly dissolved dolomite crystals with corroded margins seemingly floating in a poikilotopic anhydrite crystal. Anh = anhydrite.

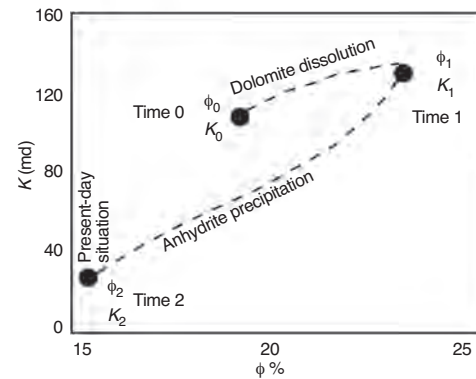
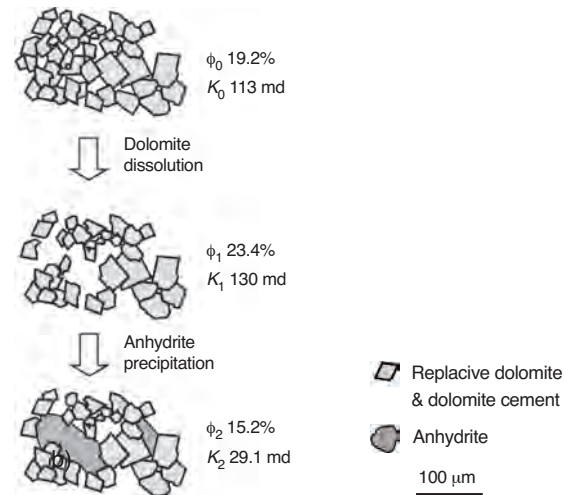


Figure 3

Schematic illustration of changes in rock fabric as a result of dissolution/precipitation processes that affected the dolostone rock. These diagenetic processes resulted in porosity-permeability modifications as illustrated at the bottom (values derived from PNM-R simulations).

size indicating a Representative Elementary Volume (REV) of  $5.4 \text{ mm}^3$  (Fig. 4). The pore (throat) size distribution obtained by mercury intrusion (Fig. 1b) indicates that with a  $\mu$ -CT resolution of  $1.5 \text{ }\mu\text{m}$ , 90% of the porosity is captured and fine intercrystalline pore connections can be imaged.

The gray scale  $\mu$ -CT images show four different constituents (Fig. 5a), i.e. from black to white: air in pores, dolomite, anhydrite and celestine. Although four constituents can be visually distinguished, the gray scale histogram shows only three peaks (Fig. 5b). Gray scale contrasts are successfully improved and the image is smoothed by applying a “mean” filter in ImageJ (i.e. each pixel is replaced by its neighbourhoods mean). Volumetric percentages of each phase, calculated after segmentation, are listed in Table 2. The resolved porosity of 16% approaches the lab measurement (18.5%) with 90% of the porosity captured, as expected.

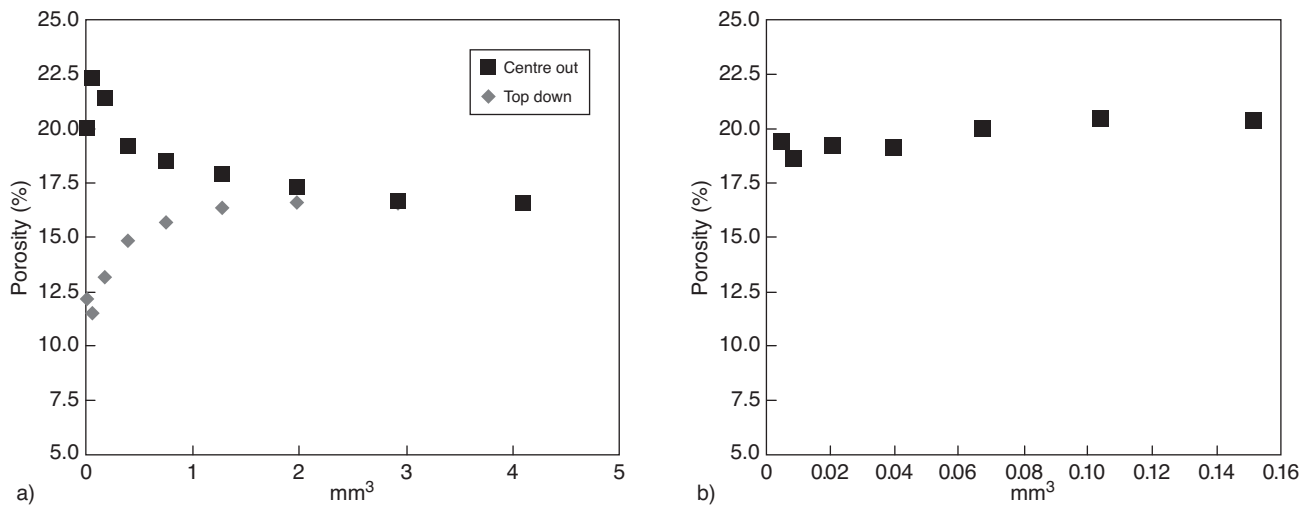


Figure 4

Calculation of visible porosity% for increasing volumes to investigate the representative elementary volume of the studied sample.

a) Time 2 - reconstructed volume  $1000 \times 1000 \times 1000$  pixels,  $1.5 \mu\text{m}$  resolution. The two curves represent two sampling schemes for the volumes: increasing volumes around the centroid and volumes increasing downwards from the upper surface of the dataset;

b) Investigation of representative elementary volume for porosity in the smaller box used to reconstruct the pore space at time 0 (max  $0.16 \text{ mm}^3$ ,  $1.5 \mu\text{m}$  resolution).

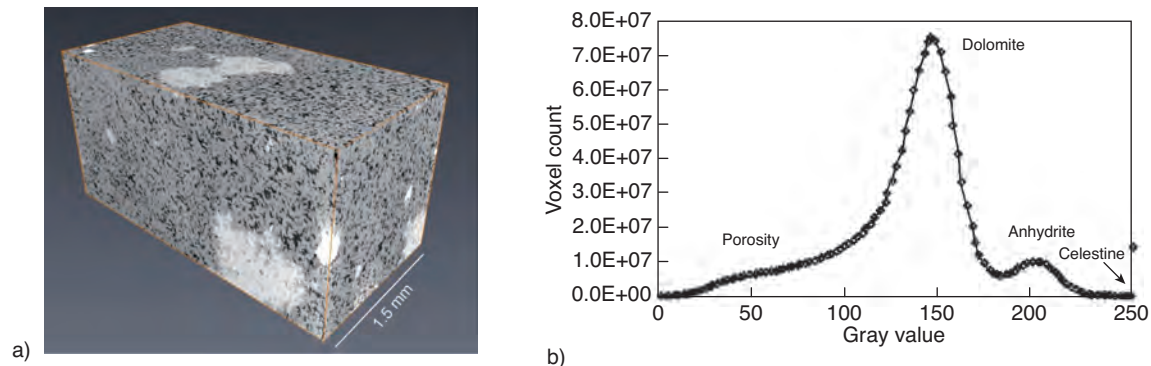


Figure 5

a) 3D gray scale view of  $\mu\text{-CT}$  scan ( $2000 \times 1000 \times 1000$  pixels); b) Gray level histogram.

TABLE 2

$\mu\text{-CT}$  quantification results for the dolostone sample.  
XRD = X-ray diffraction

	Dolomite	Anhydrite	Celestine	Total porosity	Volume percolating cluster
Vol.%	74.8	8.1	1.1	16.0	15.3
Wt%	88.2	10.0	1.8		
XRD wt%	95.4	3.6	1.0		

Visual evaluation of the segmentation is satisfactory, though the volumetric percentages of dolomite, anhydrite and celestine differ slightly from those experimentally measured by XRD on adjacent plug material (Fig. 1, Tab. 2).

Different steps of the pore network building procedure are illustrated in Figure 6. The segmented pore space shows an important percolating cluster that constitutes 95% of the total resolved porous volume. The cluster encloses the largest, connected porous volume and is further used in the reconstruction of an equivalent 3D pore network for transport property simulations. The quality of the partitioning is appreciated qualitatively and validated quantitatively through the comparison between simulated and measured petrophysical properties. First, mercury injection curves are compared. The simulated curve is in good agreement with the experimental values (Fig. 7). Not the entire curve could be reproduced as the 10% smallest pores fall below the CT resolution. In a second and more sensitive step, the permeability value is

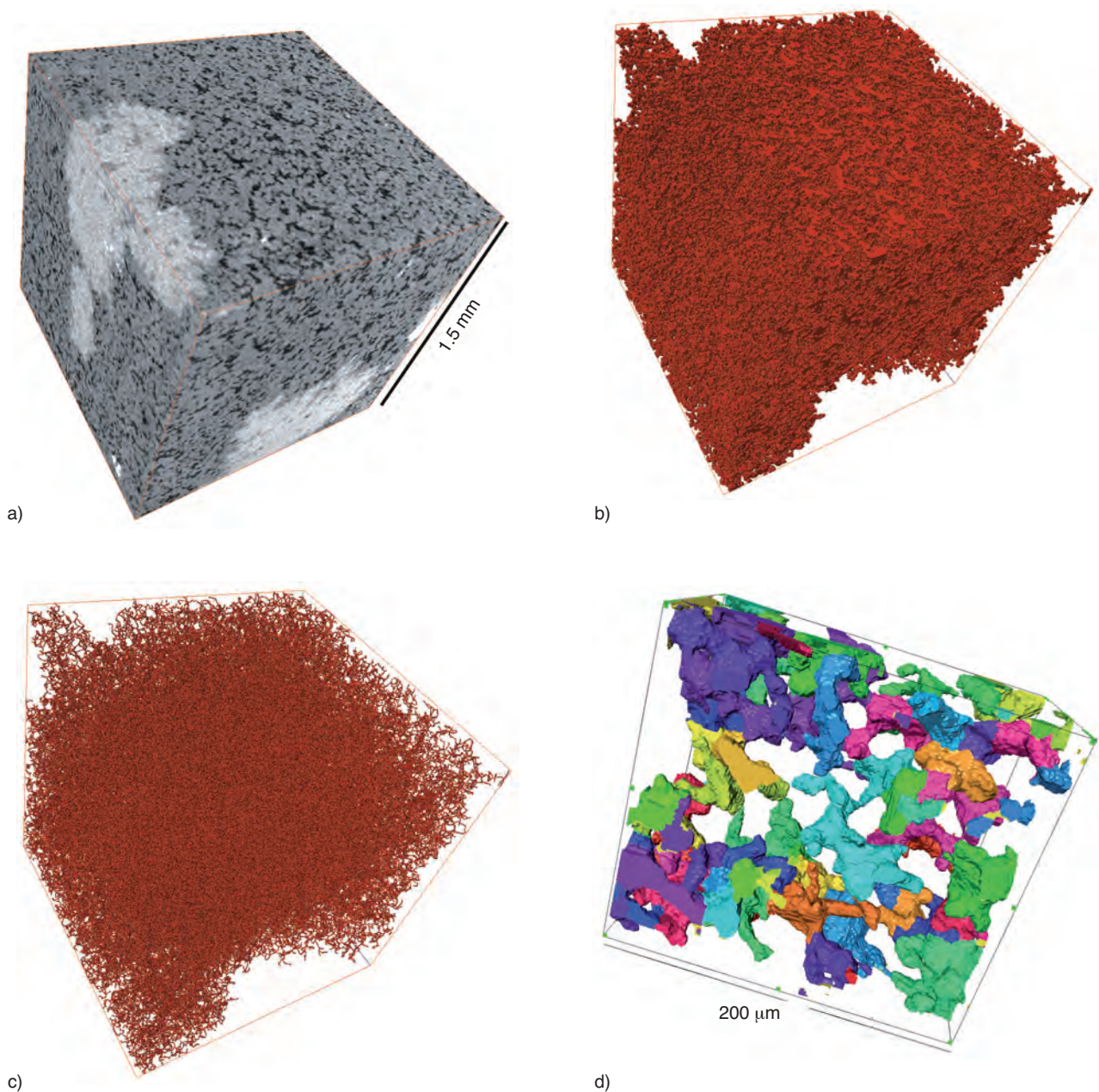


Figure 6

Equivalent network building of the present-day pore structure (time 2). a) 3D-gray scale view of  $\mu$ -CT scan ( $1000 \times 1000 \times 1000$  pixels); b) Segmented image with porosity in red, following binarisation step; c) 3D skeleton representation as lines in the center of pores, preserving the original pore topography; d) Enlarged view of part of the partitioned pore space. Each separate pore has a color distinct from its neighbouring pores.

calculated from the equivalent network yielding a value of 29.1 md, very similar to the experimental value of 31.0 md measured on a 23 mm diameter core plug.

Following the pore partitioning step, statistics on the pore size and pore connectivity are calculated, which can aid in a quantitative 3D rock fabric description. The pore size distribution is shown in Figure 8 as a frequency distribution.

Pore radius refers to the radius of a volume-equivalent sphere of the pore. The pore size distribution shows a main peak for radii between 10 and 16  $\mu\text{m}$ , corresponding to the intercrystalline porosity. No pores with a radius larger than 35  $\mu\text{m}$  were reconstructed. When comparing to the pore throat size distribution, pore radii are about 2.5 to 4 times larger than the most frequent pore throat radii. The pore coordination number refers

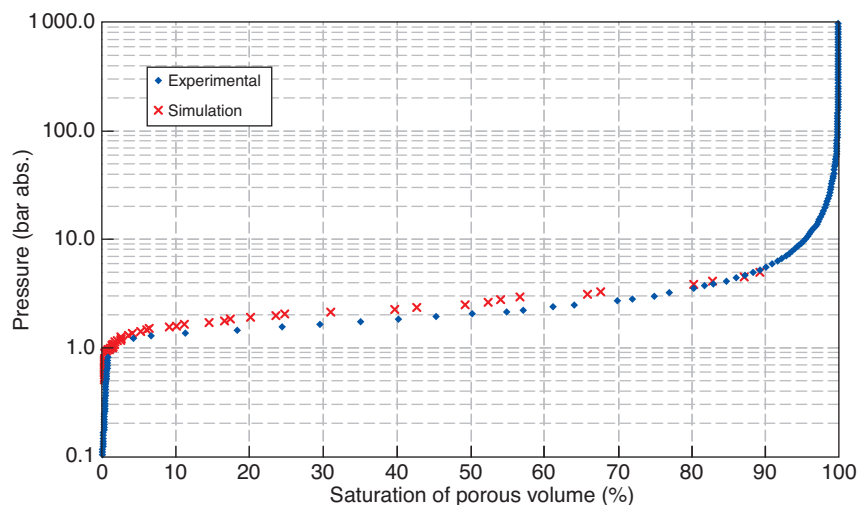


Figure 7

Simulated and measured mercury injection capillary pressure curve for the present-day pore structure (time 2).

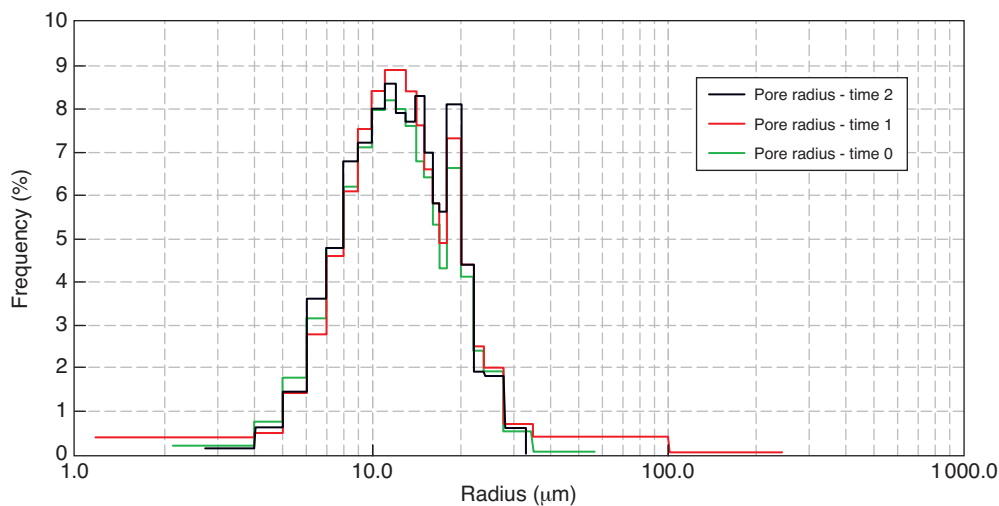


Figure 8

Pore size distribution (in % of number of pores) for the three studied time steps: time 0 to time 2 (Fig. 3). Radius refers to the radius of a sphere with equivalent volume for the pore sizes.

to the number of channels that connect to a specific pore. The pore coordination number distribution is illustrated in Figure 9 and shows that coordination 3 is the most common, but coordination numbers exceeding 10 occur. No trend is apparent between pore sizes and the pore coordination numbers.

### 3.3 Ancient Pore Networks

Following the successful reconstruction of the present pore space and simulation of its transport properties, equivalent pore networks have been reconstructed at former diagenetic

steps as fluids, like hydrocarbons, might have migrated through varying pore networks, throughout the diagenetic history. The different diagenetic steps that are addressed here are illustrated in Figure 3 together with their calculated porosity and simulated permeability characteristics. Time 0 represents the original, intercrystalline pore structure following dolomitisation. Time 1 refers to the pore structure following dolomite dissolution, prior to anhydrite cementation/replacement. Time 2 refers to the actual pore structure following anhydrite replacement and cementation. Results of the latter time step are outlined in the previous section.

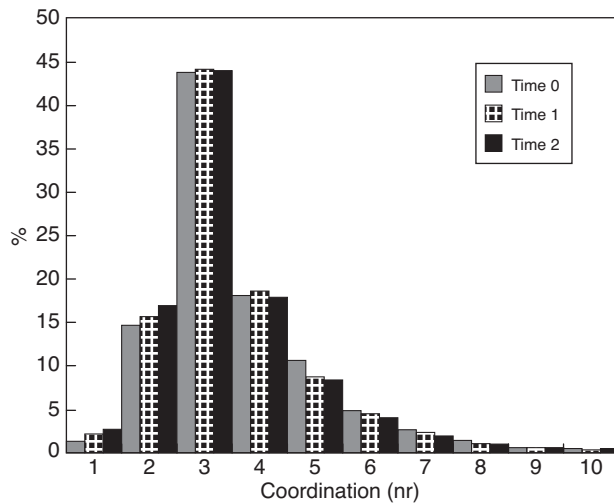


Figure 9

Frequency of coordination numbers for the three studied time steps 0 to 2.

The intercrystalline pore structure at time 0 is approached by subselecting smaller volumes (0.11 and 0.21 mm<sup>3</sup>), thereby avoiding the presence of anhydrite/celestine and the possible interference of anhydrite replacement. The porosity% was calculated for increasing volumes to verify the REV. The porosity% changes only slightly with increasing volume and volumes larger than 0.07 mm<sup>3</sup> were found to be representative (Fig. 4b). The reconstructed image should however be regarded as an approximation as it is impossible to account for the effect of late dissolution events. The calculated porosity values of 19.8 and 17.0% (Tab. 3) are slightly higher than the present-day porosity values (16%). More than 91% of the time 0 pore space makes up a percolating pore cluster that is suitable for permeability calculations. The simulated permeability of 113 md is higher than the present sample permeability (31 md) and suggests better pore connectivity for a similar porosity value. The pore size distribution is comparable to the present-day situation, but smaller pores with radii <14 μm are more common (Fig. 8).

TABLE 3

μ-CT quantification results for time step 0 and 1

	Volume	Total porosity	Percolating cluster	Simulated permeability
Time 0				
Subvolume 1	0.21 mm <sup>3</sup>	19.8%	19.2%	113 md
Subvolume 2	0.11 mm <sup>3</sup>	17.0%	15.4%	
Time 1	6.0 mm <sup>3</sup>	25.5%	23.4%	130 md

The pore structure at time 1, following dissolution, is reconstructed by considering the volume of anhydrite and celestine as pore space. The calculated porosity value for a double 2 000 × 1 000 × 1 000 volume shows an increase to 25.5%, compared to the porosity at time 0. When anhydrite and celestine are considered pore space, part of dolomite, entirely enclosed by anhydrite, becomes unconnected to the main rock. To allow the reconstruction of a porous network at time step 1, those “floating” volumes of dolomite have to be considered as porous space. These operations yield an approximation of the connected porous space at time 1 with a largest percolating cluster porosity of 23.4%. The segmented pore volume, the pore structure skeleton and the partitioned pore space figures show a network of smaller, intercrystalline pores connecting larger, “vuggy” pores (Fig. 10). The pore size distribution (Fig. 8) demonstrates the presence of few larger pores with diameters of more than 35 μm, up to 242 μm. The distribution of the coordination numbers however remains nearly identical for all the studied time steps. In spite of an important increase in porosity, the simulated sample permeability changes only slightly (130 md). It should be noted that upon reconstruction of the pore structure at time 1, all anhydrite is turned into porosity and partial anhydrite replacement of dolomite crystals could not be taken into account. As a result, the total amount of porosity increase, created by “dolomite dissolution” is overestimated.

### 3.4 PNM-R: Simulation of Changes in Petrophysical Properties During Diagenesis

The reactive pore network simulations presented here involve the initial network (time 0: before dolomite dissolution) through the different steps of diagenesis (Fig. 3). The time 0 pore network counts roughly one tenth of the number of nodes present in the two other networks at time 1 and time 2. As a consequence, computing time and instabilities due to complex network configurations are largely reduced by using the time 0 pore network as a starting point. This approach implies that, at time 1, the network used to start the anhydrite precipitation step will be the network obtained at the end of the dolomite dissolution step (Fig. 11).

During each step of the simulated diagenetic evolution, the reaction regime is fixed by the afore-mentioned dimensionless numbers of Peclet and Peclet-Damköhler. The transport-reaction regime that operated through the three diagenetic steps can already be roughly assessed by looking at the respective porosity and permeability values for the three steps that were quantified and simulated using the reconstructed 3D pore networks from each time step. The petrophysical properties found for time 0 and time 1 reveal a reduced rise of permeability for a significant rise of porosity (Fig. 3, 11a). It suggests that during the first step, dissolution occurred preferentially in the pore bodies rather than in the pore throats. Between time 1 and time 2 (Fig. 11b), the drop

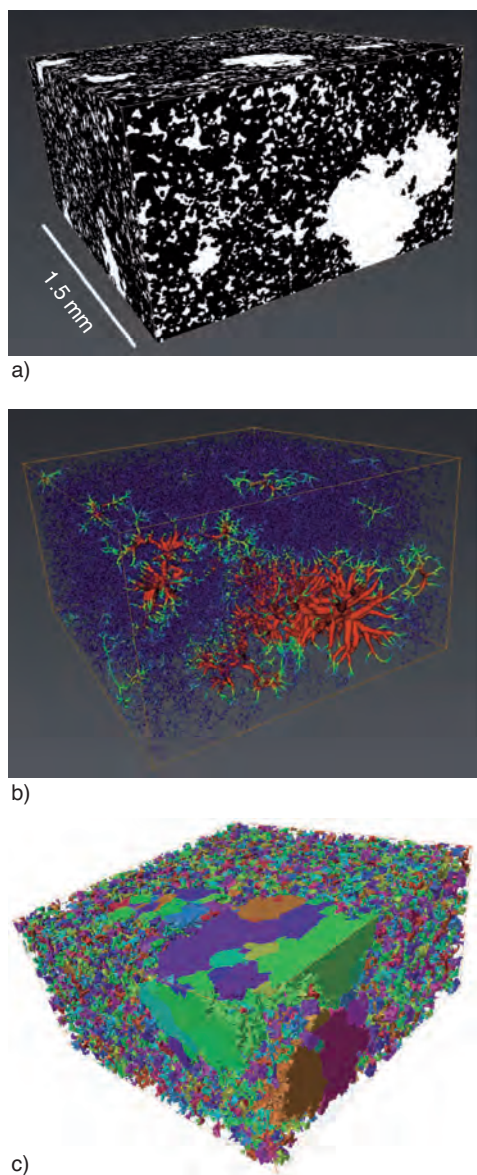


Figure 10

Equivalent network building for time step 1, prior to anhydrite cementation. a) Porosity in white following image binarisation; b) 3D skeleton representation with assigned minimum distance to the porosity border. Color gradation from blue to red with increasing pore radius; c) Detail of the partitioned pore space showing the dual porosity system at this time step. Vuggy pores are well connected with the rest of the pore system. Each separate pore has a color distinct from its neighbouring pores.

of permeability is impressive. It suggests that precipitation could have taken place uniformly, but certainly in pore throats.

The latter observations form the start for several runs to seek plausible reactive transport regimes that operate during

the dissolution step and the precipitation step. Advective flow rates used in the geochemical simulations are between 0.002 and 0.5 m/y (based on Whitaker *et al.*, 2004). It is therefore reasonable to assume that the flow is governed by diffusion rather than by convection. The following numerical study is therefore limited to Peclet numbers ( $Pe$ ) lower than 1. The Peclet-Damköhler number ( $PeDa$ ) is assumed to be low as well because of the slowness of chemical reactions in the given geological situation.

At first, we investigated the appropriate regime of dissolution to evolve from the porosity-permeability values at time 0 to the petrophysical properties of time 1 (Fig. 11a). During this first step, several couples of  $Pe$  and  $PeDa$  numbers have been tested. A PNM-R simulation for a Peclet number of 0.1 and a Peclet-Damköhler of 0.01 returns the end point closest to the simulated porosity-permeability values for the time 1 equivalent pore network (Sect. 3.3). The porosity-permeability path for this reactive-flow regime in Figure 11a indicates a minor increase in permeability for the given porosity change. This pattern points to dissolution preferentially in pore bodies and not in pore throats. Such a phenomenon was indeed expected after analysing pore size distributions of the time 1 pore network, based on the  $\mu$ -CT images (Fig. 8). It should however be born in mind that, as outlined above, time 1 is, in part a fictive end step of the dissolution process.

The simulations of the anhydrite precipitation step start from the end point of the previous step, *i.e.* using the pore network obtained at the end point of the dolomite dissolution step. Any end point of the dissolution step, close to the expected porosity and permeability could have been taken as starting point. The choice of this particular starting point has little influence on the simulation results because of the similarity of the pore size distributions and the localisation of the dissolution. During this second step, fewer couples of  $Pe$  and  $PeDa$  have been tested (Fig. 11b). In fact, instabilities occurred while simulating the precipitation phase due to clogged pore throats that modify the main flow path. Even for the completed paths, it can be noticed that most porosity-permeability curves show a similar change in gradient (“bump”), which indicates a modification of the main flow path. When the main flow path changes, the chemical disequilibrium field is modified and causes a radical change in the regime of precipitation. The results show that only one run has reached porosity values comparable to the expected 15.2% of the time 2 pore network (Sect. 3.2) with a permeability sufficiently close to the expected one. When taking a closer look at the pore size distribution after precipitation, precipitation took place along the main flow path in connected larger pore bodies, but never totally clogged big pore bodies as seen in  $\mu$ -CT images. Furthermore, small pore bodies and pore throats are (nearly) closed, explaining the important permeability drop. However, instabilities during simulation must be solved before further information can be obtained.

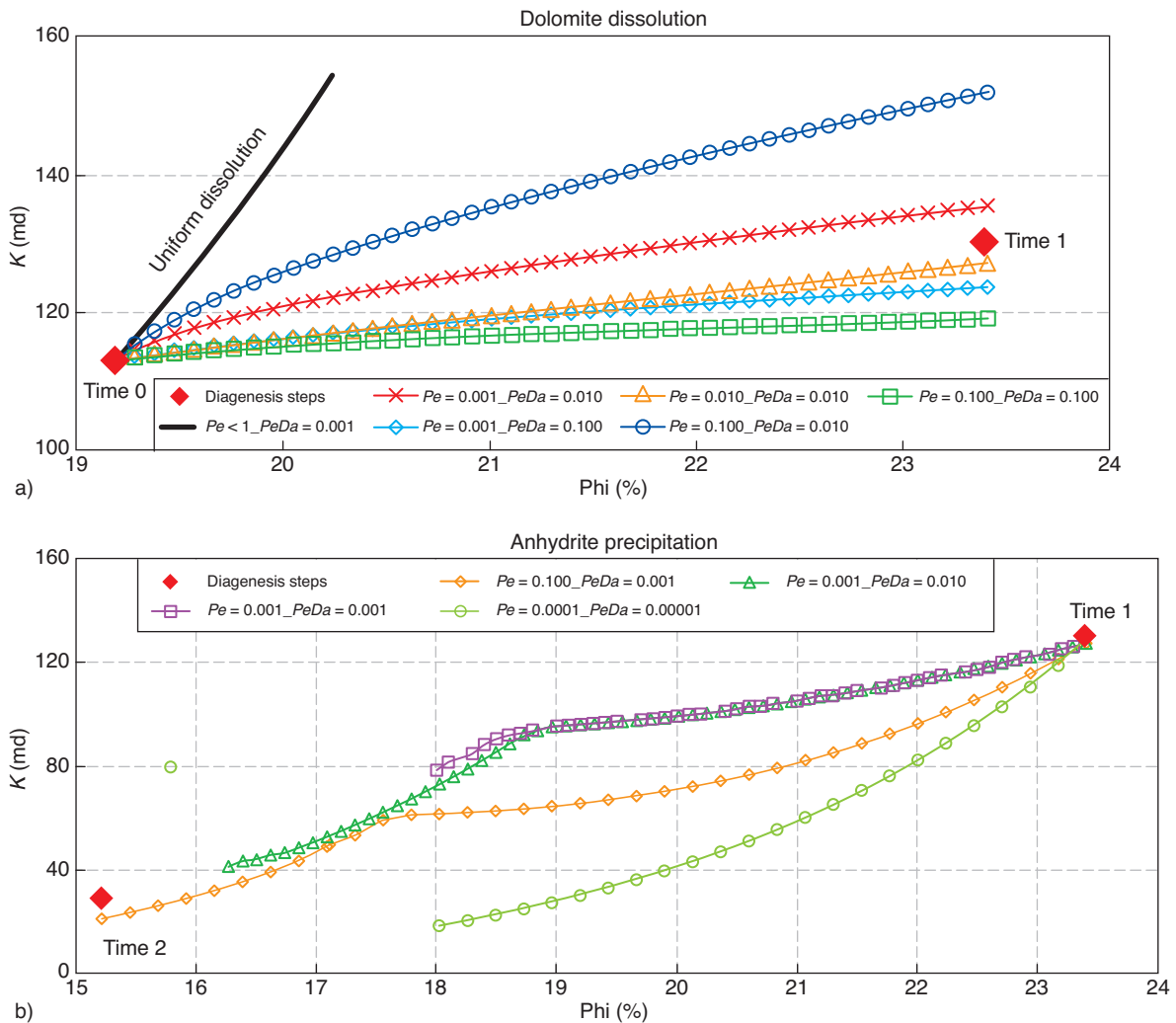


Figure 11

Porosity-permeability paths for different Peclet ( $Pe$ ) and Peclet-Damköhler ( $PeDa$ ) numbers in the case of dolomite dissolution a) and anhydrite precipitation b). See Equation (2) and (3) for equation of  $Pe$  and  $PeDa$  respectively. The dimensionless  $Pe$  number is a measure for convection versus diffusion; the  $PeDa$  number is a measure for diffusion versus reaction times.

### 3.5 Reaction Path Modeling

Table 1 lists the chemical compositions of the waters used in the geochemical simulations. Table 4 shows the chemical and physical input parameters that are varied during the different simulations. Two diagenetic processes were simulated, *i.e.* dolomite dissolution and anhydrite cementation. For each process, the burial conditions and geological framework are first defined, based on former, elaborate diagenetic work on the studied lithologies. Secondly, the results of the different simulations are discussed.

Quantitative estimation of porosity before and after dolomite dissolution shows a maximum porosity increase

of 7%. We assume a depth between 2.4 and 2.6 km, temperatures of 85° to 95°C and a maximum duration of about 40 My (Gasparini, pers. comm.). At this moment the Arab Formation became buried as a result of the formation of fault thrusts and the emplacement of the Oman ophiolites (Alsharhan, 1989). From oil-bearing inclusions in replacive dolomite, it is clear that oil-bearing fluids from depth were allowed to migrate upwards to the Arab Formation, prior to anhydrite cementation (Gasparini, pers. comm.). The geological situation probably favoured faulting and could allow the migration of fluids related to the maturation of organic matter, present in *e.g.* the Diyab Formation (Upper Jurassic; Alsharhan, 1989) to migrate upward rapidly. A scenario is

TABLE 4

Chemical and physical input parameters that are varied during different reaction path simulations. My = million years, SI = saturation index

Dolomite dissolution (time 0 to time 1)		
Porosity change	7%	
Grain radius dolomite	50 $\mu\text{m}$	
Duration event	unknown (assume 40 My)	
Flow velocity	0.5 m/y	
CO <sub>2</sub>	0.015 (mol/kg)	0.050 (mol/kg)
Cooling	$\Delta T = 10^\circ$	
Temperature	85°C	95°C
SI calcite	-0.39	-0.03
SI dolomite	-0.43	-0.16
SI anhydrite	-0.13	0.01
Anhydrite cementation (time 1 to time 2)		
Porosity change	9%	
Grain radius dolomite	50 $\mu\text{m}$	
Grain radius anhydrite	300 $\mu\text{m}$	
Duration event	40 My	
Flow velocity	2 mm/y	
SO <sub>4</sub> <sup>2-</sup>	0.07 (mol/kg)	
Ca <sup>2+</sup>	0.005 (mol/kg)	
Na <sup>+</sup>	2.82 (mol/kg)	3.42 (mol/kg)
Cl <sup>-</sup>	3.3 (mol/kg)	3.7 (mol/kg)
Temperature	95°C	105°C
SI calcite	-0.34	-0.13
SI dolomite	0.04	0.22
SI anhydrite	-0.24	0

therefore examined in which dolomite dissolution is related to an increase in CO<sub>2</sub> in solution and possibly the cooling of upward migrating formation waters. The simulation temperature and CO<sub>2</sub> concentration are varied (Tab. 4), to address the variability of the results. The results indicate a duration of 18 000 to 36 000 years to complete 7% of dolomite dissolution. The concentration of CO<sub>2</sub> in solution (0.015 to 0.05 mol/kg; pH of 4.8 to 6.6) plays a major role and is capable of halving the total, estimated reaction duration. In addition, a one order increase in fluid velocity can decrease the duration to dissolve 7% of dolomite by one order. It is well-known that dolomite is characterized by a reverse solubility. The cooling of a fluid equilibrated with the host rock at 95°C, to 85°C has, however, only a minor impact and this cooling effect is insufficient on its own to dissolve sufficient dolomite in the given time frame. Under conditions of high concentrations of CO<sub>2</sub> in solution, Ca<sup>2+</sup> ions released in solution upon dolomite dissolution lead to anhydrite oversaturation.

Following fault activity, overpressure diffuses rapidly within 10 to 100 years (Appold *et al.*, 2007). This would indicate that to dissolve 7% of dolomite in the studied

rock, 1 800 to 3 600 fault events might have been necessary (calculated total duration, divided by 10 years), or a faulting recurrence time of several tens of thousands years. This is not unrealistic and supports the simulated scenario.

The dissolution of dolomite was followed by, but probably also contemporaneous with, anhydrite precipitation. Fluid inclusion studies indicate that anhydrite formed at temperatures between 95° to 105°C (depth: 2.6 to 2.9 km), implying a maximum time period of 40 My based on the burial curve (Gasparrini, pers. comm.). At this moment, tectonic uplift and compression remain important and might have influenced fluid migration in the basin. Porosity decreases from 25% to 16% during anhydrite plugging. Two scenarios are investigated. At first, the end fluid following dolomite dissolution at 95°C is used to simulate anhydrite precipitation. The reaction is however too slow and concurrent dissolution of dolomite causes a net increase in porosity. In a second case, an increase in salinity, *i.e.* Na<sup>+</sup>, Cl<sup>-</sup> concentration, is imposed on the sulphate- and Ca<sup>2+</sup>-rich pore water composition. This might relate to interaction of pore waters with evaporitic deposits. The simulations indicate a slow reaction and a long time necessary to complete this diagenetic step between 6 My and 13 My. An increase in salinity together with an increase in the temperature of reaction (95° to 105°C) has the largest impact on the calculated reaction duration. The assumed, low fluid flow velocity (0.05 m/y) and limited anhydrite oversaturation of the input fluid explain the important duration of this diagenetic step.

The presented geochemical simulations provide an estimate of the reaction rate in m<sup>3</sup>/s, *i.e.* the dissolved (or precipitated) mineral volume (m<sup>3</sup>) in a given time (s). The calculated reaction rates are constant over time. The volume must be divided by the reactive surface area to obtain the correct, intrinsic reaction rate constant ( $\kappa$ , m/s) used in the *PeDa* expression (Eq. 3). Values for  $\kappa$  (m/s) are between 1 and  $3 \times 10^{-18}$  for dolomite dissolution and between 1 and  $8 \times 10^{-20}$  for anhydrite precipitation.

## 4 DISCUSSION

### 4.1 Approach for Quantitative Diagenesis

The presented approach allows quantifying the rocks' components and a realistic description of the geometry of the 3D pore structure. A good agreement can be achieved between porosity and quantitative XRD measurements, and the  $\mu$ -CT image-based quantification results for a representative sample subvolume. Further validation of the reconstructed 3D pore network by comparison of simulated and measured absolute permeability and Mercury Injection Capillary Pressures (MICP) shows a good agreement, subscribing the applied methodology to reconstruct the 3D pore structure and simulate its transport properties (Youssef *et al.*, 2007b).

Besides the simulation of actual, petrophysical rock properties, this study goes one step further. It demonstrates an approach to approximate and quantitatively describe ancient 3D pore structures starting from  $\mu$ -CT images. Moreover, the equivalent pore networks extracted for relevant diagenetic steps serve as input for Pore Network Models (PNM) that can quantify the petrophysical properties at these time steps. This allows us to move in time and approximate the transport characteristics of realistic reservoir rocks at specific key moments in their diagenetic evolution. The approach therefore prepares the ground for an accurate and full description of rock-types evolving throughout early and late diagenetic events that shape the quality of a reservoir rock.

#### 4.2 Towards the Prediction of Dynamic Petrophysical Properties During Diagenesis

Reactive-PNMs furthermore allow simulating the continuous evolution of transport properties during pore structure modifications for different reactive-transport scenarios. As such, PNM-Rs provide a promising tool to define plausible scenarios for the evolution of pore structure and petrophysical characteristics during diagenetic processes, providing insight in how different rock-types tend to evolve one into another.

Qualitative and quantitative comparison with  $\mu$ -CT observations,  $\mu$ -CT-derived pore size distributions, and the geochemical simulation results allow interpreting and comparison with the PNM-R simulations. Geochemical parameters can be used to guide the choice of appropriate dimensionless Peclet ( $Pe$ ) and Peclet-Damköhler ( $PeDa$ ) numbers for PNM-R (see Eq. 2, 3). At first, it is possible to define the Peclet number from the flow velocities defined in the geochemical model (Tab. 4). This yielded a number of Peclet in the order of  $10^{-5}$  for the dolomite dissolution step (Fig. 11a) with the diffusion parameter  $D$  about  $10^{-9}$  m<sup>2</sup>/s,  $l$  of 4  $\mu$ m and  $v$  in the order of 0.02  $\mu$ m/s (Eq. 2). The low Peclet number suggests that transport is chiefly governed by diffusion and not by convection. In the case of the anhydrite precipitation step, the Peclet number is in the order of  $10^{-7}$ . Its even lower value is due to the lower flow velocities that were assumed for this diagenetic step (Tab. 4).

For the first step,  $PeDa$  is varied between 0.01 and 0.1 ( $\kappa$ :  $10^{-4}$  to  $10^{-5}$  m/s) in the PNM-R simulations, while for the second step, simulations were conducted for smaller  $PeDa$  between 0.01 and 0.0001 as a result of the lower  $\kappa$  values ( $10^{-5}$  to  $10^{-8}$  m/s). As outlined in Section 3.5, an idea of the  $PeDa$  number during the dissolution and precipitation reactions can also be gained from the reaction path simulation results. Unfortunately, the  $\kappa$  and thus  $PeDa$  calculated from the geochemical simulation results are not coherent and very much lower (lower than  $10^{-8}$ ) compared to the  $\kappa$  values of the scenarios in PNM-R.

It is necessary to point out, at this stage that the geochemical reaction path simulations are bound by numerous assumptions

that affect the calculated reaction rates. The most important parameters that affect the latter are:

- the kinetic constants, derived from (extreme) laboratory dissolution experiments far from equilibrium (factor  $10^2$  to  $10^3$ ; Palandri *et al.*, 2004);
- the thermodynamic model used for fluid speciation (factor up to  $10^5$  when changing from the Pitzer model to Debye-Hückel);
- changes in the assumed fluid velocity (factor  $10^2$ ; Sect. 2.4);
- the reactive grain surface in contact with the solution (<factor 10; Sect. 2.4);
- the composition of the aqueous solution (maximum factor 10), which is difficult to assess correctly for ancient diagenetic steps, and;
- dissolution and precipitation events were simulated separately while they were at least partly linked during anhydrite replacement of dolomite. Even taking these uncertainties into account, the geochemically modeled diagenetic reactions remain slow, compared to the reactive transport scenarios that were simulated by the reactive pore network models to go from one end point to the next in Figure 3.

The low, geochemical reaction rates, and thus low  $PeDa$  values, obtained by geochemical simulations imply uniform and reversible reaction over the whole network in the reactive pore network model. To illustrate such a scenario, a uniform dissolution/deposition cycle was simulated starting from the time 0 network. When looking in more detail to the dolomite dissolution step, it is likely that the reaction was indeed more homogeneous. As anhydrite replacement of dolomite crystals *versus* anhydrite cementation in pores can not be quantified, the porosity created during the dolomite dissolution step is overestimated. The porosity at time 1 therefore most probably plots at lower values (see arrow and green diamond in Fig. 12). When starting the precipitation step from a point close to the gray curve in Figure 12, a uniform precipitation indeed fits with expected porosity and permeability at time 2 and is in better agreement with the geochemical scenario.

However, when evaluating qualitatively the distribution of anhydrite in the rock sample, anhydrite tends to be concentrated in nodules. So, visual observations indicate that anhydrite precipitation was probably favoured in some places. To reproduce such a heterogeneous distribution in PNM-R simulations, a much higher  $PeDa$  (and  $\kappa$ ) value would be required. This second incoherence between qualitative observations, geochemical simulations and the PNM-R results might reveal a problem of the PNM-R approach in its present form. The PNM-R in its actual form does not account for the possibility that the location of precipitation/dissolution phenomena in nature might be favoured at some places as a result of the diagenetic history of the pore surface or the presence of nucleation sites. To address this effect of preferential reaction at

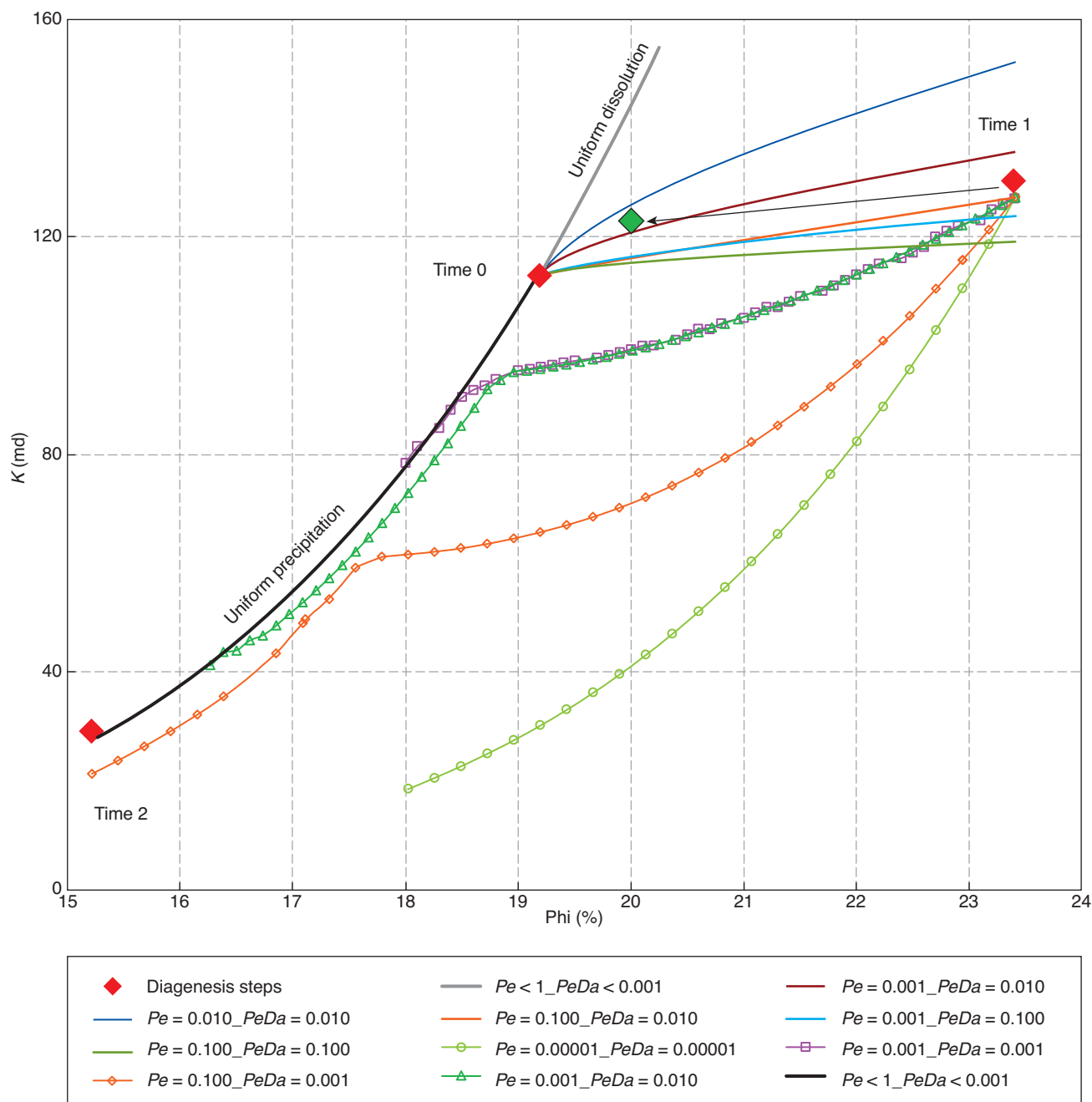


Figure 12

Porosity-permeability paths for different Peclet ( $Pe$ ) and Peclet-Damköhler ( $PeDa$ ) for the two diagenetic steps investigated. The dimensionless  $Pe$  number is a measure for convection *versus* diffusion; the  $PeDa$  number is a measure for diffusion *versus* reaction times. An additional, gray and black curve indicates the path for uniform dissolution and precipitation respectively, both starting from the time 0 network. The green diamond between time 0 and time 1 marks the position of a hypothetical time 1 “end point”, in case anhydrite replacement could be accounted for in the workflow.

given places, on the pore structure and porosity-permeability properties, a test could be conducted in which two different (low)  $\kappa$ 's are introduced in the PNM-R for different pore bodies and throats in the network.

In addition, the present diagenetic scenarios that were simulated by PNM-R start from the assumption that porosity and permeability properties evolved continuously along a single path between two end points. Petrographic observations

suggest that anhydrite is partly replacive with respect to the dolomite phases. At present, we cannot simulate porosity-permeability property changes for precipitation and dissolution processes (*i.e.* replacement) taking place at the same time. In order to better approach the porosity-permeability changes during the process of anhydrite replacement, alternative scenarios should be tested. A first test could be the simulation of multiple (nearly uniform) precipitation – dissolution events that alternate in time and, on a geological time scale, might reflect the replacement process of anhydrite *versus* dolomite.

Following this discussion, current challenges of this study are to verify:

- the application to other case studies with different degrees of heterogeneity and a pluri-modal pore size distribution, possibly including the presence of microporosity (Knackstedt *et al.*, 2006; Youssef *et al.*, 2008);
- the use of representative stochastic networks in PNM-R to reduce instabilities and computation time. PNM-R computations can then provide macroscopic numbers at the core scale (see Algive, 2009b) to help in improving reactive transport modeling during reservoir studies. As for the pore scale, macroscopic coefficients representing apparent reaction rate, velocity vector and dispersive tensor of the solute can be defined. Thus, in integrating a macroscopic advection-dispersion equation similar to Equation (1) in a reservoir model, the concentration field can be determined at this scale while taking into account surface reaction at the pore scale.

## CONCLUSION

A dolostone reservoir rock (Jurassic Arab Formation, Arabian Gulf region) was subjected to an integrated approach to quantify changes in pore structure and predict the evolution of petrophysical properties throughout its diagenetic history:

- classical 2D microscopy shows that processes that affected the reservoir quality are porosity enhancement by dolomite dissolution and porosity destruction by cementation of late anhydrite;
- X-ray  $\mu$ -CT imaging permits the 3D quantification of the volume and distribution of the different sample constituents. The quantification results are in satisfying agreement with experimental He-porosity and quantitative XRD measurements. The reliability of the reconstructed 3D pore network is furthermore validated by comparing permeability and mercury injection capillary pressure measurements with values obtained by pore network transport simulations. A good agreement was found for both parameters;
- to go back in time and investigate the porosity-permeability characteristics of ancient pore networks, characterizing former diagenetic steps, a Pore Network Model (PNM) was applied. The results suggest a porosity increase, with

the creation of some larger (vuggy) pore bodies, but a limited change in permeability following dolomite dissolution. An important drop in both parameters is observed after anhydrite plugging of large pore bodies, but also fine pore bodies and throats;

- to simulate complete porosity-permeability paths during the dolomite dissolution step and subsequent anhydrite precipitation step, reactive pore network models (PNM-Rs) are applied. The final porosity-permeability values of each simulation are compared with the simulated porosity-permeability characteristics of the  $\mu$ -CT derived pore networks. Good approaches can be found for both steps;
- geochemical modeling provides dissolution/precipitation reaction rates and flow velocities, taking into account the geological history and a realistic geochemical environment. Comparisons with equivalent PNM-R model parameters, however, indicate important differences. Problems arise from the fact that the used  $\mu$ -CT-derived pore networks are an approximation of the real networks at former diagenetic steps. Secondly, the reaction rates obtained from geochemical simulations (low Peclet-Damkohler numbers) are very low and would lead to homogeneous instead of heterogeneous anhydrite precipitation in the PNM-R simulations.

This study shows that the combination of a classical diagenetic study with  $\mu$ -CT imaging, PNM(-R) and geochemical simulation results could provide a tool for quantitative rock-typing of reservoir rocks and can be a first step in the direction of numerical modeling of diagenetic processes and subsequent dynamic rock-typing.

## ACKNOWLEDGMENTS

The authors would like to thank IFP Energies nouvelles for the permission to publish these results. The two reviewers are greatly acknowledged for their useful comments that helped to improve the manuscript.

## REFERENCES

- Algive L., Békri S., Lerat O., Nader F.H., Vizika O. (2009a) Reactive pore network modeling technology to evaluate the impact of diagenesis on the petrophysical properties of a rock, *Paper IPTC 14049* presented at the *International Petroleum Technology Conference*, Doha, Qatar, 7-9 December.
- Algive L., Békri S., Vizika O. (2009b) Reactive pore network modeling dedicated to the determination of the petrophysical property changes while injecting CO<sub>2</sub>, *SPE Paper 124305* presented at the *SPE Annual Technical conference and Exhibition*, New Orleans, Louisiana, USA, 4-7 October.
- Alsharhan A.S. (1989) Petroleum geology of the United Arab Emirates, *J. Petrol. Geol.* **12**, 3, 253-288.
- Appold M.S., Garven G., Boles J.R., Eichhubl P. (2007) Numerical modeling of the origin of calcite mineralization in the Refugio-Careros fault, Santa Barbara Basin, California, *Geofluids* **7**, 79-95.

- Bemer E., Lombard J.M. (2010) From injectivity to integrity studies of CO<sub>2</sub> geological storage, *Oil Gas Sci. Technol. - Revue IFP* **65**, 3, 445-459.
- Brosse E., Magnier C., Vincent B. (2005) Modelling fluid-rock interaction induced by the percolation of CO<sub>2</sub>-enriched solutions in core samples: the role of reactive surface area, *Oil Gas Sci. Technol. - Revue IFP* **60**, 2, 287-305.
- Cantrell D.L., Hagerty R.M. (2003) Reservoir rock classification, Arab-D reservoir, Ghawar field, Saudi Arabia, *GeoArabia* **8**, 3, 435-462.
- Christman P.G., Edgar T.F. (1983) Distributed pore size model for sulfatation of limestone, *Am. Institute Chem. Eng.* **29**, 3, 388-395.
- Coelho A.A. (2007) *Topas Academic v4.1*, <http://members.optusnet.com.au/~alancoelho/>.
- Ehrenberg S.N. (2006) Porosity destruction in carbonate platforms, *J. Petrol. Geol.* **29**, 1, 41-52.
- Ehrenberg S.N., Nadeau P.H., Aqrabi A.A.M. (2007) A comparison of Khuff and Arab reservoir potential throughout the Middle East, *AAPG Bull.* **91**, 3, 275-286.
- Fatt I. (1965) The network model of porous media, *The American Institute of Mining, Metallurgical and Petroleum Engineers Transactions* **207**, 144-181.
- Izgec O., Zhu D., Hill A.D. (2010) Numerical and experimental investigation of acid wormholing during acidization of vuggy carbonate rocks, *J. Petrol. Sci. Eng.* **74**, 51-66.
- Knackstedt M.A., Arns C., Ghouse A., Sakellariou A., Senden T., Sheppard A.P., Sok R.M., Averdunk H., Pinczewski W.V., Pady G.S., Ioannidis M.A. (2006) 3D imaging and flow characterization of the pore space of carbonate core samples, *Paper SCA2006-23* presented at the *International Symposium of Core Analysts*, Trondheim, Norway, 12-16 September.
- Laroche C., Vizika O. (2005) Two-phase flow properties prediction from small-scale data using pore-network modeling, *Transport Porous Med.* **61**, 77-91.
- Li L., Peters C.A., Celia M.A. (2006) Upscaling geochemical reaction rates using pore-scale network modeling, *Adv. Water Resour.* **29**, 1351-1370.
- Lindsay R.F., Cantrell D.L., Hughes G.W., Keith T.H., Mueller H.W., Russell S.D. (2006) Ghawar Arab-D reservoir: widespread porosity in shoaling-upward carbonate cycles, Saudi Arabia, in *Giant hydrocarbon reservoirs of the world: from rocks to reservoir characterization and modeling*, AAPG Memoir 88/SEPM Special Publication, Harris P.M., Weber L.J. (eds), pp. 97-137.
- Lønøy A. (2006) Making sense of carbonate pore systems, *AAPG Bull.* **90**, 9, 1381-1405.
- Lucia F.J. (2007) *Carbonate reservoir characterization - An integrated approach*, 2nd edition, Springer-Verlag Berlin Heidelberg, pp. 336.
- Meyer F.O., Price R.C. (1992) A new Arab-D depositional model, Ghawar field, Saudi Arabia, *SPE Paper* 25576, 1-10.
- Mitchell J.C., Lehmann P.J., Cantrell D.L., Al-Jallal I.A., Al-Thagafy M.A.R. (1988) Lithofacies, diagenesis and depositional sequence; Arab-D Member, Ghawar field, Saudi Arabia, in *Giant Oil and Gas Fields - A Core Workshop*, Lomando A.J., Harris P.M. (eds), Society of Economic Palaeontologists and Mineralogists, Core Workshop No. 12, 459-514.
- Moldovanyi E.P., Walter L.M. (1992). Regional trends in water chemistry, Smackover Formation, southwest Arkansas: Geochemical and physical controls, *AAPG Bulletin* **76**, 6, 864-894.
- Morad S., Al-Aasm I.S., Nader F.H., Ceriani A., Gasparini M. (accepted) Diagenesis impact on the spatial and temporal distribution of reservoir properties in C and D Members of the Arab Formation (Jurassic), *GeoArabia*.
- Palandri J.L., Kharaka Y.K. (2004) A compilation of rate parameters of water-mineral interaction kinetics for application to geochemical modeling, USGS Report.
- Pitzer K.S. (1973) Thermodynamics of electrolytes. I. Theoretical basis and general equations, *J. Phys. Chem.* **12**, 268-277.
- Rieckmann C., Frerich K. (1997) Multicomponent diffusion and reaction in three-dimensional networks: General kinetics, *Ind. Eng. Chem. Res.* **36**, 8, 3275-3281.
- Schechter R.S., Gidley J.L. (1969) The change in pore size distribution from surface reactions in porous media, *Am. Institute Chem. Eng.* **15**, 3, 339-350.
- Snellings R., Machiels L., Mertens G., Elsen J. (2010) Rietveld refinement strategy for quantitative phase analysis of partially amorphous zeolitized tuffaceous rocks, *Geologica Belgica* **13**, 3, 183-196.
- Swart P.K., Cantrell D.L., Westphal H., Robertson Handford C., Kendall C.G. (2005) Origin of dolomite in the Arab-D reservoir from the Ghawar field, Saudi Arabia: Evidence from petrographic and geochemical constraints, *J. Sediment. Res.* **75**, 3, 476-491.
- Whitaker F.F., Smart P.L., Jones G.D. (2004) Dolomitization: from conceptual to numerical models, in *The Geometry and petrogenesis of dolomite hydrocarbon reservoirs*, *Geological Society of London, Special Publications* 235, Braithwaite C.J.R., Rizzi G., Darke G. (eds), pp. 99-139, London.
- Wood W.W., Sanford W.E., Rahman S.A.I. Habshi A. (2002). Source of solutes to the coastal sabkha of Abu Dhabi, *GSA Bulletin* **114**, 3, 259-268.
- Youssef S., Han M., Bauer D., Rosenberg E., Bekri S., Fleury M., Vizika O. (2008) High resolution  $\mu$ -CT combined to numerical models to assess electrical properties of bimodal carbonates, *Paper SCA 2008 - Temp Paper#A54* presented at the *International Symposium of Core Analysts*, Abu Dhabi, UAE, 29-30 October.
- Youssef S., Rosenberg E., Gland N., Bekri S., Vizika O. (2007a) Quantitative 3D characterisation of the pore space of real rocks: improved  $\mu$ -CT resolution and pore extraction methodology, *Paper SCA 2007-17* presented at the *International symposium of the Society of Core Analysts*, Calgary, Canada, 10-12 September.
- Youssef S., Rosenberg E., Gland N., Skalinski M., Vizika O. (2007b) High resolution CT and pore-network models to assess petrophysical properties of homogeneous and heterogeneous carbonates, *Paper SPE 111427* presented at the *SPE/EAGE Reservoir Characterization and Simulation Conference*, Abu Dhabi, U.A.E., 28-31 October.

Final manuscript received in July 2011  
Published online in February 2012

Copyright © 2012 IFP Energies nouvelles

Permission to make digital or hard copies of part or all of this work for personal or classroom use is granted without fee provided that copies are not made or distributed for profit or commercial advantage and that copies bear this notice and the full citation on the first page. Copyrights for components of this work owned by others than IFP Energies nouvelles must be honored. Abstracting with credit is permitted. To copy otherwise, to republish, to post on servers, or to redistribute to lists, requires prior specific permission and/or a fee: Request permission from Information Mission, IFP Energies nouvelles, fax. +33 1 47 52 70 96, or [revueogst@ifpen.fr](mailto:revueogst@ifpen.fr).